First publ. in: Applied Physics / A, Materials Science and Processing, 66 (1998), Supplement 1, pp. S1007-S1011

Imaging of dopants in surface and sub-surface layers of the transition metal dichalcogenides WS_2 and WSe_2 by scanning tunneling microscopy

Th.W. Matthes[2], Ch. Sommerhalter[2], A. Rettenberger[1], P. Bruker[1], J. Boneberg[1], M.Ch. Lux-Steiner[2], P. Leiderer[1]

[1] University of Konstanz, Physics Department, Universitätsstr.10, D-78434 Konstanz, Germany
[2] Hahn-Meitner-Institut Berlin, Glienicker Str. 100, D-14109 Berlin, Germany
(Fax: +49-30/8062-3199, E-mail: Matthes@hmi.de)

Received: 25 July 1997/Accepted: 1 October 1997

Abstract. The van-der-Waals surfaces (0001) of the layered structure semiconductors WS_2 and WSe_2 are known to be free of intrinsic surface states. Therefore, they provide an ideal system for investigations of the influence of individual dopants on the local electronic properties, which can be measured by scanning tunneling microscopy (STM). Individual dopant sites were resolved as topographic depressions superimposed on the atomically resolved lattice. The apparent depth of these depressions showed a discrete statistical distribution and was attributed to the spatial depth of the dopant site. Using an STM-induced electrochemical process, we could locally expose the first and second sub-surface layer to correlate the previously recorded topographic contrast to the location of buried dopants. To our knowledge this is the first direct proof of the capability of STM to detect individual sub-surface dopants. An interpretation of the contrast mechanism is given in terms of tip-induced band-bending effects and current transport mechanisms involving minority charge carrier injection and majority charge carrier extraction.

Scanning tunneling microscopy can be used to directly image the dopant distribution on semiconductor surfaces or interfaces. This is an important application with respect to microelectronics, where efforts are made to minimize device structures to the nm scale. For that purpose doping distributions have to be controlled with high spatial resolution. In order to use the STM as a reliable tool for device characterization, the basic topographic and spectroscopic contrast mechanisms observed in the vicinity of individual dopant sites have to be investigated. In the case of semiconductor surfaces with a high density of surface states in the forbidden band gap (such as Si(111)7×7), the electronic properties are governed by surface states. As a result of screening effects impurities may solely contribute to a lateral contrast on the atomic scale. In contrast semiconductor surfaces with a low density of intrinsic surface states may show a topographic contrast within several nm in the vicinity of an individual dopant site due to localized charges and band-bending effects.

Most of the STM investigations concerning dopants in semiconductors were reported for highly doped GaAs(110) [1–10]. Superimposed on the atomically resolved lattice, topographic contrasts with lateral dimensions of several nm were observed and attributed to localized dopant sites.

The contrast (topographic depression or hillock) was shown to depend on the sample voltage and type of doping. Cox et al. [1] attributed depressions in the topographic image to As vacancies in p-GaAs (negative sample voltage) and Ga vacancies in n-GaAs (positive sample voltage). Feenstra et al. [2–4] showed that arsenic antisite defects (i.e. As on Ga sites) result in hillocks with variable heights, which they correlated to the spatial depth of the defect for the first time. Johnson et al. [5, 6] showed that Be and Zn acceptors also result in hillocks in p-type GaAs (negative sample voltage). They calculated the topographic contrast by assuming a scattering process for holes, involving the ionized acceptor, while depressions observed for Al [6] in p-GaAs were explained by the energetic position of Al states in the conduction band of GaAs. Zheng et al. [7, 8] showed that Zn acceptors in p-type GaAs and Si donators in n-type GaAs result in hillocks independent on the applied sample voltage and also claimed a possible depth resolution. Goldman et al. [9] investigated GaAs/GaN superlattices and attributed topographic depressions to N on As sites.

Concerning the transition metal dichalcogenides semiconductors MX_2 (M = Mo,W; X = Se,S), rather few results exist. Various structures such as hillocks, depressions, ring structures or dark and bright atomic spots have been reported [11–15]. Reviews are given by Whangbo et al. [13] and Maganov et al. [14, 15]. However the authors were not able to experimentally relate the different observations to the chemical nature of the investigated dopants and their STM measurements were performed under ambient conditions, so that the influence of adsorbates and tip contamination may have played an important role. Their theoretical considerations did not include the influence of tip-induced band-bending, which we show to be essential for the MX_2(0001) surfaces [16].

In spite of the lack of reliable STM measurements concerning dopants, the transition metal dichalcogenides have the great advantage that their van-der-Waals surface (0001)

is known to be free of intrinsic surface states [17]. All chemical bonds are saturated, as adjacent covalently bound MX_2 layers are weakly coupled by van-der-Waals interactions. Doping is achieved either by adding impurities or by adjusting the chalcogenide partial pressure during crystal growth. A detailed review of the MX_2 material properties is given in [18].

In [19, 20] we show that the layered structure MX_2 semiconductors can be structured by STM and AFM under ambient conditions, involving an electrochemical etching process. In addition to reliable UHV STM measurements, our approach was to combine STM imaging under high vacuum conditions with etching under ambient conditions, to get direct insight onto dopants located in sub-surface layers, and to investigate their contribution to the topographic STM contrast.

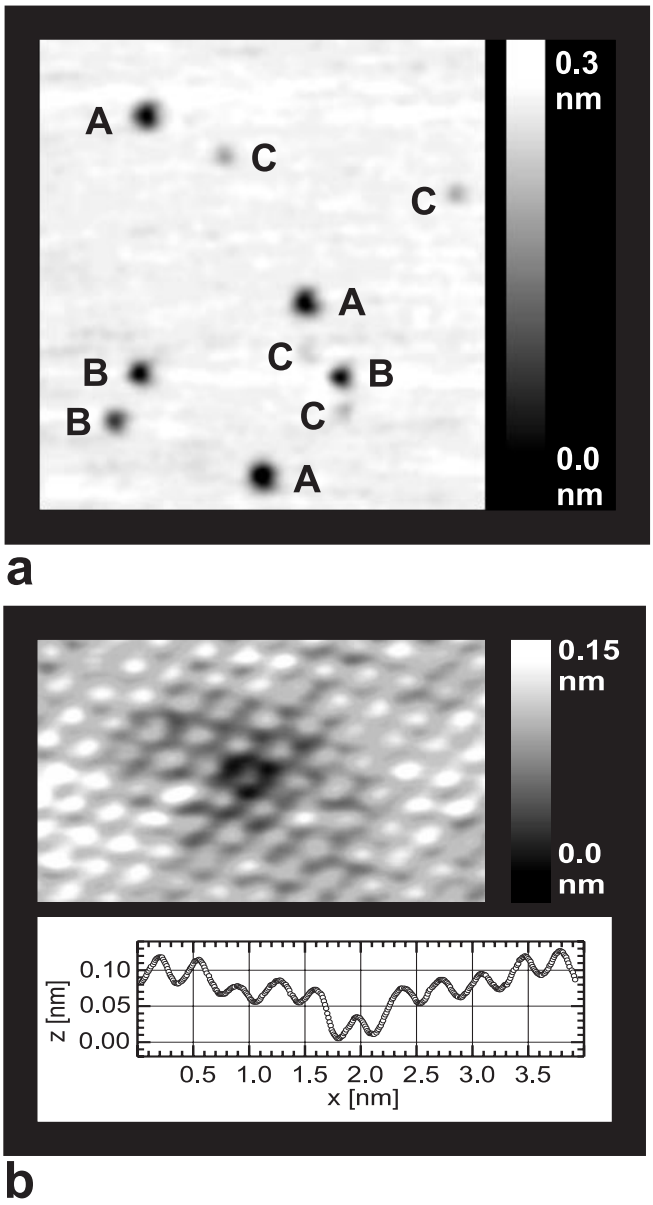

Fig. 1a,b. Topographic image of a WS_2 single crystal (0001) surface. **a** Topography acquired at $V_{sample} = 0.95$ V, $I_{ref} = 3$ nA, scan area 65 nm × 65 nm. Topographic depressions labeled A, B, C are attributed to acceptors embedded in the uppermost, first and second sub-surface molecular layers, respectively. **b** Zoom and cross-section at an acceptor site, showing the preserved atomic order within the depressions ($V_{sample} = 1.5$ V, $I_{ref} = 5$ nA, scan area 3.5 nm × 2.5 nm)

1 Experimental

For our STM investigations we used WS_2 and WSe_2 single crystals, grown by chemical vapour transport (without intentionally adding impurities, as well as with additional nickel and oxygen doping). Temperature-dependent Hall measurements showed that all samples were p-type, with charge carrier concentrations of 5×10^{16} to 2×10^{17} cm^{-3}, hole mobilities of 120–230 cm^2/Vs and activation energies of about 100 meV. To expose a clean, atomically flat (0001) surface, the crystals were either cleaved in situ or introduced immediately into the vacuum chamber after cleavage in air. The used STMs were operated in UHV (5×10^{-10} mbar) or in a high-vacuum (10^{-6} mbar) chamber, which allowed fast venting and pumping without loss of the scanned area for the etching experiments.

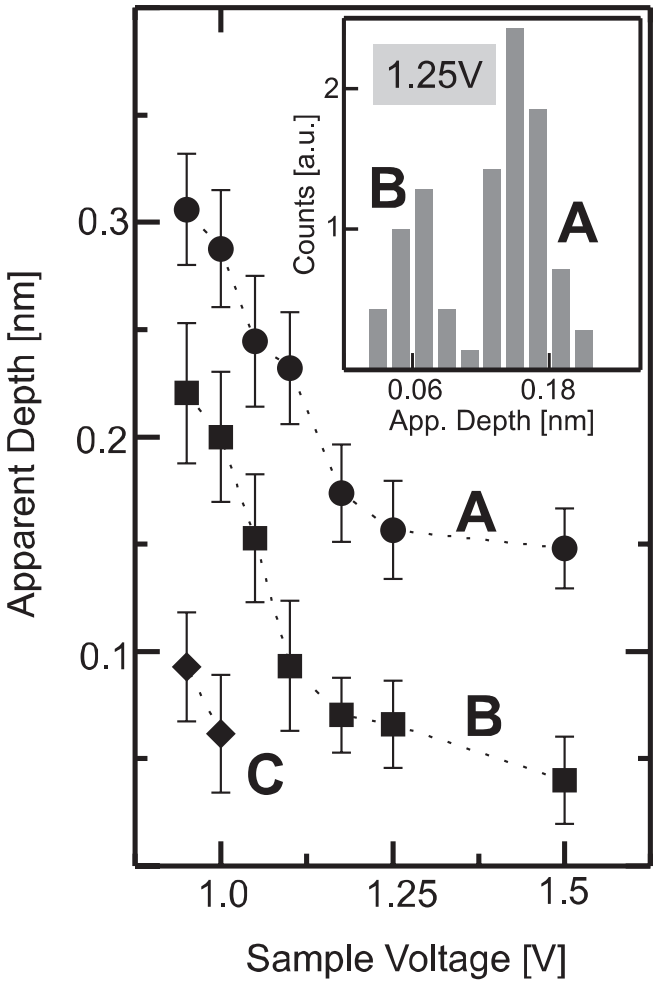

Fig. 2. Dependence of the apparent depth of the dopant-related topographic depressions (A-, B-, and C-type) on the applied sample voltage ($I_{ref} = 3$ nA). The inset shows the statistic distribution of depression depths acquired at $V_{sample} = 1.25$ V

2 Results and discussion

Figure 1a shows an STM image acquired on a WS_2 ($p = 2 \times 10^{17}\,cm^{-3}$) single crystal. Superimposed on the atomically resolved lattice (Fig. 1b), topographic depressions were observed with typical diameters in the range of 3–5 nm. The apparent depth of the observed depressions increased with decreasing sample voltage as depicted in Fig. 2. The statistical investigation of more than 100 individual depressions revealed a discrete distribution (see inset in Fig. 2 for 1.25 V).

These results indicated that as with the interpretation of the hillocks, which were reported for GaAs(110) [2–8], the observed depressions on WS_2 might be associated with acceptors embedded in the surface layer (A), first (B) or second (C) sub-surface-layer, respectively (one layer consists of one MX_2 sandwich). In order to give a direct proof for this interpretation, we first imaged the surface of a $p = 5 \times 10^{16}\,cm^{-3}$ WSe_2 single crystal under high vacuum conditions (Fig. 3a). Then the vacuum chamber was vented with air to enable STM-induced electrochemical etching (which requires an adsorbed water layer [19, 20]). By applying short voltage pulses for initial defect nucleation and scanning at positive sample voltage of 1.5 V over selected areas, the WSe_2 could be removed layer by layer in a controlled way. After evacuation of the STM chamber and subsequent tip cleaning, the same area was imaged again (Fig. 3b–e). In the upper half of the image the first and partially the second WSe_2 layer were removed, to expose the surface of the first and second sub-surface layer. The depressions, that had been classified as B- and C-type (indicated by arrows in Fig. 3a), were now resolved to be located in the first and second sub-surface layers, respectively (The images in Fig. 3c–e correspond to Fig. 3b with the contrast adjusted to the individual layer surfaces). To our knowledge, this is the first direct proof that dopants located in sub-surface layers may contribute to the topographic contrast in STM [21]. These results also confirm the assumptions published for the GaAs(110) surface.

From the crystal growth conditions, we expected the acceptors states to be mainly caused by W vacancies. The concentration of acceptors deduced from the STM images was a factor 2–3 higher than the net charge carrier concentration determined by Hall measurements. However, the STM detects all acceptors, whereas the Hall measurement determines only thermally ionized dopants. As the majority charge carrier concentration was not in the range of carrier exhaustion at room temperature, the STM results are consistent with the macroscopic measurement.

Based upon the tunneling spectroscopy results on WS_2 [16], the influence of surface states can be neglected for the interpretation of the observed topographic contrast. Figure 4

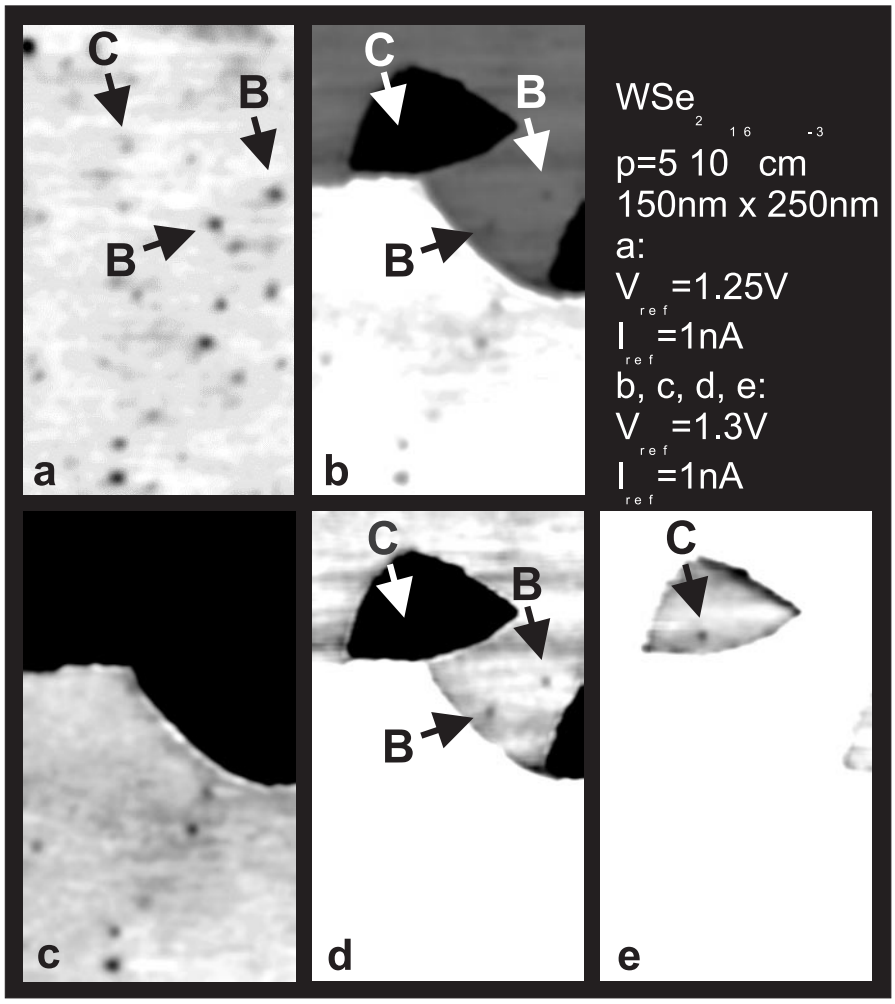

Fig. 3a–e. Topographic image of a WSe_2 single crystal before **a** and after **b–e** removal of the first and partial removal of the second WSe_2 layers in the upper half of the image. The step height is 0.6 nm. In **c–e** the image contrast is adjusted to the individual layer surfaces

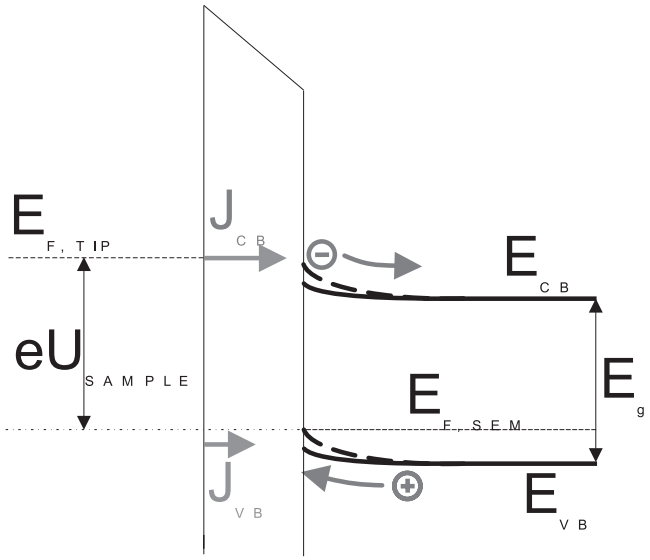

Fig. 4. Band scheme for the tunneling contact on a p-WS_2 sample for a sample voltage of 1.4 V

illustrates the principles of the underlying charge transport mechanisms. For positive sample voltages the tunneling current consists of two components, a minority injection current into the conduction band of the semiconductor (J_{CB}), and a majority extraction current from the valence band (J_{VB}). Close to an acceptor site, the tip is opposite to a higher majority concentration, and the semiconductor bands are bent further upward (indicated as dashed lines in Fig. 4). Therefore, J_{CB} is reduced while J_{VB} is increasing. As the injection current mainly determines the total tunneling current for low or moderate doping levels, the local reduction in J_{CB} causes the tip to approach the surface to maintain constant current. The increase of the apparent depth with decreasing sample voltage is caused by the fact that the additional local barrier inside the semiconductor (dashed line in Fig. 4) shows a stronger influence on the total minority injection current for lower sample voltages.

The reverse topographic contrast (hillock) is expected, and was also measured, for highly doped semiconductors [2–8]. In the case of high doping levels, the majority extraction dominates the tunneling current.

Under ambient conditions, we observed that the depressions, measured under high vacuum and UHV conditions, in general were imaged as hillocks, which is consistent with results in [13–15]. This observation is also evident from the model given above. Under ambient conditions the gap between tip and sample is likely to consist of a water film. An extension of the simple electrostatic model in [16] to the case of a dielectric tip/sample gap ($\varepsilon_{water} \approx 80$!) shows that the system then essentially behaves like a Schottky diode. Therefore, the majority current dominates for moderate and low doping levels as well. Even the ring structures reported in [11–15] may be explained by the competing current contribution of minority injection and majority extraction. Current investigations using standard and photoassisted scanning tunneling spectroscopy strengthen the validity of the description given above, and will be published in a forthcoming paper.

Topographic images of oxygen-doped and nickel-doped WSe_2 are shown in Fig. 5. As well as topographic depressions, which extended over several nm and were observed in comparable concentrations as for the samples above, these crystals also exhibited strongly localized structures on an atomic scale, which we attribute to the different chemical bonding in the vicinity of the impurities. The strong lateral localization indicates, that the O and Ni impurities do not act as active dopants, as no additional charge accumulation was detected on a scale of several nm as described before. In addition, the impurity concentration observed by STM was too high ($10^{20}\,cm^{-3}$) to be compatible with the net charge carrier concentrations and activation energies determined by Hall measurement. This also allows to conclude that O and

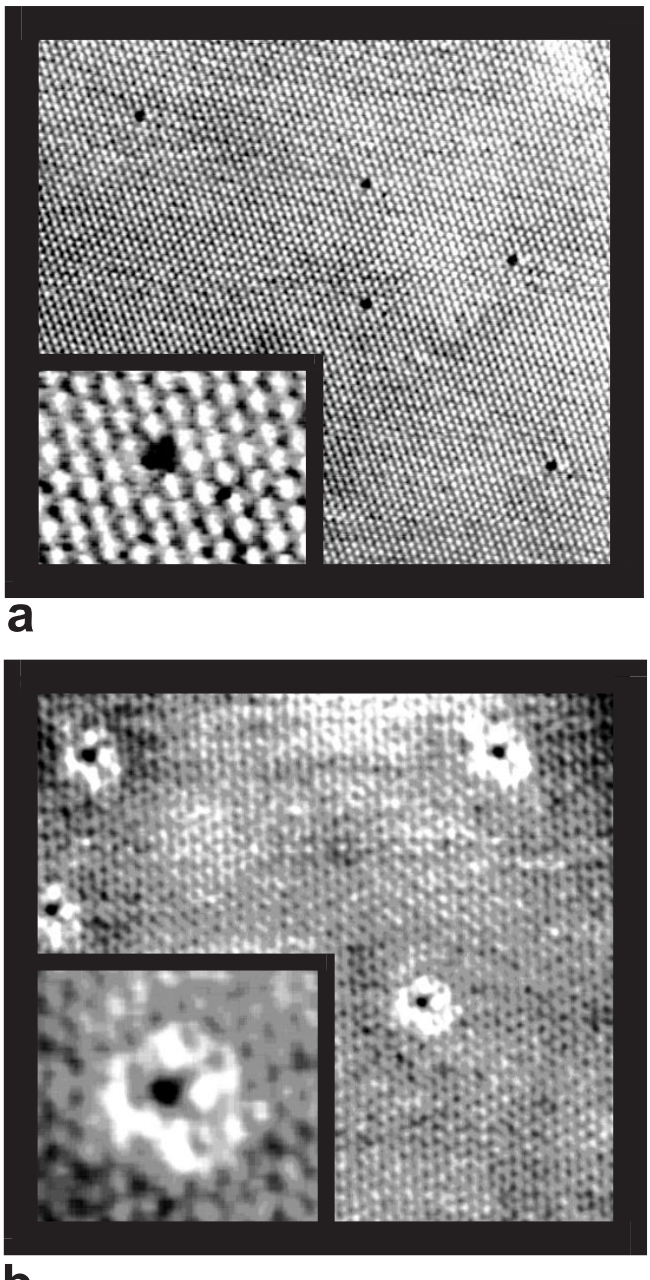

Fig. 5. a (0001) surface of an O-doped p-WSe_2 crystal. ($V_{sample} = 1.3$ V, $I_{ref} = 1$ nA, scan area 20 nm × 18 nm). **b** (0001) surface of an Ni-doped p-WSe_2 crystal. ($V_{sample} = 1.4$ V, $I_{ref} = 3$ nA, scan area 15 nm × 13 nm)

Ni impurities do not significantly influence the charge carrier concentrations in WSe_2.

3 Conclusions

We performed STM investigations of dopants in WS_2 and WSe_2 single crystals. We could directly demonstrate that the discrete distribution in the apparent depth of topographic depressions is correlated with the localization of acceptors in the first, second and third molecular layer. This is the first direct proof for the capability of the STM to detect buried dopants. While the topographic depressions were attributed to W vacancies, O and Ni impurities led to strongly localized topographic structures which indicate, that O and Ni are not active as dopant and do not essentially contribute to the charge carrier concentration in WSe_2.

Acknowledgements. We gratefully acknowledge the financial support by the Deutsche Forschungsgemeinschaft (SFB 513) and the European Community (JOU2 CT93-352).

References

1. G. Cox, Ph. Ebert, K. Urban: Inst. Phys. Conf. Ser. **117**, 347 (1991)
2. R.M. Feenstra, J.M. Woodall, D.G. Petit: Phys. Rev. Lett. **71**, 1176 (1993)
3. R.M. Feenstra, A. Vaterlaus, J.M. Woodall, D.A. Collins, T. C. McGill: Mater. Res. Symp. **332**, 15 (1994)
4. R.M. Feenstra, J.M. Woodall, G.D. Petit: Mater. Res. Forum **143-147**, 1311 (1994)
5. M.B. Johnson, O. Albrektsen, R.M. Feenstra, H.W.M. Salemink: Appl. Phys. Lett. **63**, 2923 (1993)
6. M.B. Johnson, M. Pfister, S.F. Alvarado, H.W.M. Salemink: Mater. Res. Soc. Symp. Proc. **332**, 598 (1994)
7. J.F. Zheng, X. Liu, N. Newman, E.R. Weber, D.F. Ogletree, M. Salmeron: Phys. Rev. Lett. **72**, 1490 (1994)
8. Z.F. Zheng, M.B. Salmeron, E.R. Weber: Appl. Phys. Lett. **64**, 1836 (1994)
9. R.S. Goldman, R.M. Feenstra, B.G. Briner, M.L. O'Steen, R.J. Hauenstein: Appl. Phys. Lett. **69**, 3698 (1996)
10. M.C.M.M. van der Wielen, A.J.A. van Roij, H. van Kempen: Phys. Rev. Lett. **76**, 1075 (1996)
11. W.A. Heckl, F. Ohnesorge, G. Binnig, M. Specht, M. Hashimi: J. Vac. Sci. Technol. B **9**, 1072 (1991)
12. Th. Schimmel, H. Fuchs, S. Akari, K. Dransfeld: Appl. Phys. Lett. **59**, 1039 (1991)
13. M.H. Whangbo, J. Ren, S.N. Maganov, H. Bengel, B.A. Parkinson, A. Suna: Surf. Sci. **326**, 311 (1995)
14. S.N. Magonov, M.-H. Whangbo: *Surface analysis with STM and AFM* (VCH, Weinheim 1996) and references therein
15. S.N. Maganov, H.J. Cantow, M.H. Whangbo: Surf. Sci. **318**, L1175 (1994)
16. Ch. Sommerhalter, Th.W. Matthes, J. Boneberg, M.Ch. Lux-Steiner, P. Leiderer: J. Vac. Sci. Technol. B **15**, 1876 (1997)
17. T. Mayer, A. Klein, O. Lang, W. Jaegermann: Surf. Sci. **269**, 909 (1991) and references therein
18. A. Aruchamy: *Photoelectrochemistry and photovoltaics of layered semiconductors* (Kluwer Academic Press, Netherlands 1992)
19. J. Boneberg, M. Lohrmann, M. Böhmisch, F. Burmeister, M.Ch. Lux-Steiner, P. Leiderer: Z. Phys. B **99**, 567 (1996)
20. M. Böhmisch, F. Burmeister, J. Boneberg, P. Leiderer: Appl. Phys. Lett. **69**, 1882 (1996)
21. Recently we have learned that similar observations have been made in the group of B. Parkinson CSU, Fort Collins, but have not been published